

RBM20和MURC双基因杂合变异对心肌细胞结构和生物学特性的影响

李乔薇^{1,2,3}, 袁音^{1,2,3}, 朱文晴¹, 杨艳芳¹, 黄峰^{1,2,3}

(1. 福建医科大学省立临床医学院老年医学科, 福州 350001; 2. 福州大学附属省立医院老年医学科, 福州 350001; 3. 福建省临床老年病研究所, 福州 350001)

摘要 目的 探讨RNA结合基元蛋白20 (RBM20) 和肌肉相关卷曲螺旋蛋白 (MURC) 双基因杂合变异对人心肌细胞AC16 (成人左心室心肌细胞系) 结构和生物学特性的影响。方法 构建对照组、空载组、野生组、MURC或RBM20单基因突变组、RBM20和MURC双基因突变组的心肌细胞AC16; 采用Western blotting、免疫荧光染色和实时荧光定量PCR观察心肌细胞中RBM20和MURC定位、细胞表面积、骨架排列、骨架相关蛋白、细胞极性、细胞内钙浓度; 采用流式细胞术检测心肌细胞凋亡; 采用Ki-67染色检测心肌细胞增殖; 采用划痕实验检测心肌细胞迁移。结果 与RBM20或MURC单基因突变相比, RBM20和MURC双基因突变对心肌细胞结构和生物学特性影响更显著, 表现为细胞表面积增大, 细胞肥大相关基因肌球蛋白重链7和 α 肌动蛋白基因mRNA表达升高, 骨架排列紊乱度升高, 骨架蛋白 β -tubulin和Vinculin荧光强度降低 (均 $P < 0.01$); 极性蛋白Part6荧光强度升高 ($P < 0.05$); 心肌细胞凋亡率升高, 增殖活性下降, 迁移率增高, 细胞内钙离子浓度升高 (均 $P < 0.01$)。结论 RBM20和MURC双基因杂合变异使心肌细胞结构及生物学特性发生改变, 表现为细胞表面积增大, 骨架排列紊乱, 极性改变, 凋亡率和迁移率升高, 增殖活性和钙处理能力降低。

关键词 RNA结合基元蛋白20; 肌肉相关卷曲螺旋蛋白; 双基因杂合变异; 心肌病

中图分类号 R542.2 文献标志码 A 文章编号 0258-4646(2024)10-0882-11

网络出版地址 <https://link.cnki.net/urlid/21.1227.R.20241009.1600.010>

DOI: 10.12007/j.issn.0258-4646.2024.10.004

Effect of RBM20 and MURC digenic heterozygosity variation on the structure and biological characteristics of myocardial cells

LI Qiaowei^{1,2,3}, YUAN Yin^{1,2,3}, ZHU Wenqing¹, YANG Yanfang¹, HUANG Feng^{1,2,3}

(1. Department of Geriatric Medicine, Shengli Clinical Medical College of Fujian Medical University, Fuzhou 350001, China; 2. Department of Geriatric Medicine, Fuzhou University Affiliated Provincial Hospital, Fuzhou 350001, China; 3. Fujian Institute of Clinical Geriatrics, Fuzhou 350001, China)

Abstract Objective To investigate the impact of variations in RNA-binding motif protein 20 (RBM20) and muscle-restricted coiled-coil (MURC) digenic heterozygosity variation on the structural and biological characteristics of human cardiomyocyte AC16 (an adult left ventricular myocardial cell line). **Methods** Cardiomyocyte AC16 cell lines were constructed with control, negative scramble, wild-type, MURC single-gene mutant, RBM20 single-gene mutant, and RBM20 and MURC digenic mutant groups. The localization of RBM20 and MURC in cardiomyocytes, cell area, cytoskeletal arrangement, cytoskeleton-related proteins, cell polarity, and intracellular calcium concentration were observed using Western blotting, immunofluorescence staining, and reverse transcription polymerase chain reaction. Myocardial apoptosis was detected using flow cytometry. Ki-67 staining and wound healing assays were performed to detect cardiomyocyte proliferation and migration, respectively. **Results** Digenic mutations had a more pronounced impact than single-gene mutations in RBM20 or MURC on the structural and biological characteristics of cardiomyocytes, manifested by increased cell area, upregulated mRNA expression of hypertrophy-related genes, such as myosin heavy chain 7 and alpha-actin, increased cytoskeleton disturbance, decreased fluorescence intensity of cytoskeletal proteins β -tubulin and Vinculin (all $P < 0.01$); increased fluorescence intensity of the polarity protein Part 6 ($P < 0.05$); and significantly elevated cardiomyocyte apoptosis rate, decreased proliferative activity, and elevated migration rate and intracellular calcium ion concentration (all $P < 0.01$). **Conclusion** The digenic heterozygous variation in RBM20 and MURC may induce changes in the morphological structure and biological characteristics of myocardial cells, including increased cell area, cytoskeleton disturbance, cell polarity, increased apoptosis rate and mobility, decreased cell proliferation activity, and calcium processing ability.

基金项目: 福建省自然科学基金重点项目(2020J02058); 福建省科技创新联合资金项目(2023Y9276)

作者简介: 李乔薇(1988-), 女, 主治医师, 博士。

通信作者: 黄峰, E-mail: wmhf0327@126.com

收稿日期: 2024-01-18

网络出版时间: 2024-10-10 14:39:12

Keywords RNA-binding motif protein 20; muscle-restricted coiled-coil; digenic heterozygosity variation; cardiomyopathy

课题组前期研究^[1]发现1例心肌结构异常伴右心室扩大的患者。Sanger测序提示受检者携带2个罕见可疑致病基因变异:RNA结合基元蛋白20(RNA-binding motif protein 20, *RBM20*)基因c.224C>T杂合变异和肌肉相关卷曲螺旋蛋白(muscle-restricted coiled-coil, *MURC*)基因c.71A>T杂合变异;患者心脏磁共振检查结果显示,左心室肌层较厚,形状正常。右心室腔扩大,肌层变薄,可见疏松的非致密化组织,肌小梁可见。疏松非致密化组织和肌小梁的出现见于心肌致密化不全(noncompaction of ventricular myocardium, NVM)。NVM是以心室内异常粗大肌小梁和交错深隐窝为特征的1种与基因相关的遗传性心肌病,发病原因尚未明确。目前,分子遗传学研究^[2]表明,30%患者NVM表型与肌节基因突变有关;其他患者与Z线、细胞骨架和线粒体基因突变有关。

*RBM20*是与心肌病相关的基因,在心脏中表达量最高。多项研究^[3-5]表明*RBM20*基因突变可直接引起心肌改变,包括心房和心室扩张,心肌广泛纤维化,肌节表面积增大,骨架结构紊乱、电生理和收缩异常,钙处理能力异常等。*MURC*作为一种Z线成分蛋白,主要在心脏中表达,其编码肌节和细胞骨架蛋白的基因突变是心肌病的主要原因^[6-7]。可见,*RBM20*或*MURC*单基因突变均能导致心肌病,表现为心脏结构和功能的改变。

目前尚无关于*RBM20*和*MURC*双基因突变报道,课题组预实验提示*RBM20*和*MURC*双基因突变会导致其蛋白质和mRNA表达下降,可能加剧对心肌的影响。本研究选择人心肌细胞AC16构建突变基因*RBM20*和*MURC*过表达体系,探讨*RBM20*和*MURC*双基因杂合变异对心肌细胞表面积、骨架、极性、凋亡、增殖、迁移和钙处理能力的影响,旨在为明确双基因变异和心肌病之间的作用机制提供新的证据,同时为临床诊疗提供指导和参考。

1 材料与方法

1.1 细胞

人心肌细胞AC16购自北京北纳创联生物技术

研究院。

1.2 主要试剂和仪器

突变*MURC*病毒液、突变*RBM20*病毒液[汉恒生物科技(上海)有限公司],*RBM20*抗体(武汉云克隆科技股份有限公司),BCA蛋白定量试剂盒(美国Thermo Fisher Scientific公司),逆转录试剂盒(日本TaKaRa公司),CCK-8检测试剂盒[上海东仁化学科技有限公司],Co-IP试剂盒(上海翎因生物科技有限公司),荧光定量PCR仪AP7500(美国Thermo Fisher Scientific公司),Western blotting电泳仪、化学发光检测仪(美国Bio-Rad公司)。

1.3 方法

1.3.1 慢病毒载体构建:构建突变的*MURC*和*RBM20*慢病毒载体和对照病毒载体的设计由汉恒生物科技(上海)有限公司按步骤完成。

1.3.2 分组:将状态良好的AC16细胞分为对照组(Control组,无干预的正常AC16细胞)、空载组(Blank组,不携带*MURC*和*RBM20*基因的慢病毒感染AC16细胞)、野生组(*MURC* WT+*RBM20* WT组,携带*MURC*和*RBM20*基因的慢病毒感染AC16细胞)、*MURC*单基因突变组(*MURC* MU+*RBM20* WT组,将携带*MURC* c.71A>T和*RBM20*基因的慢病毒感染AC16细胞)、*RBM20*单基因突变组(*RBM20* MU+*MURC* WT组,将携带*RBM20* c.224C>T和*MURC*基因的慢病毒感染AC16细胞)、*RBM20*和*MURC*双基因突变组(*MURC* MU+*RBM20* MU组,携带*MURC* c.71A>T和*RBM20* c.224C>T的慢病毒感染AC16细胞)。

1.3.3 Western blotting检测:采用BCA法测定样本蛋白浓度,样品蛋白10~25 μg/孔上样,电泳及转膜,室温封闭1 h,一抗4 ℃孵育过夜。1×TBST洗膜3次。二抗室温孵育1 h,1×TBST洗膜3次,曝光及扫描。以GAPDH为内参,采用ImageJ软件进行图像分析。

1.3.4 实时荧光定量PCR

提取心肌细胞RNA,按照PrimeSeriPt RT Reagent Kit With GDNA Eraser试剂盒说明书进行反转录和PCR扩增。引物序列:*MURC*,正向5'-TCGCATAGCA ATACAGGGCA-3',反向5'-GGACACCGAAACTTCT CCTGG-3';*RBM20*,正向5'-GCAGCCATACCCAGTA

CCC-3', 反向5'-CATTACCCCAGTGAAAGGATGC-3'。采用 $2^{-\Delta\Delta Ct}$ 法计算目的基因表达量。

1.3.5 流式细胞仪检测细胞凋亡率: 各组均加入0.25%胰酶(不含EDTA)消化细胞。取 1×10^5 个细胞悬液至流式管, 加Annexin V-PE (5 μ L) 和7-AAD (5 μ L) 混匀, 室温避光孵育15 min, 加PBS 300 μ L重悬细胞, 用流式细胞仪检测凋亡细胞。

1.3.6 Fura 2-AM检测细胞内 Ca^{2+} 浓度实验: 将6组心肌细胞接种到96孔板中, 3×10^4 孔; 将1 mL HBSS与1 μ L Fura 2-AM (0.1 μ mol/L) 于1.5 mL EP管中混合, 每孔加入50 μ L混合液培养, HBSS清洗细胞2次, 使用完全培养基孵育细胞30 min; 于高内涵镜下观察并定量分析细胞内平均 Ca^{2+} 荧光强度。

1.3.7 罗丹明标记的鬼笔环肽染色实验: 将6组心肌细胞接种到96孔板中, 将孔中完全培养基吸净, PBS (用0.5% Triton X-100 配制) 清洗3次, 4%多聚甲醛固定10 min; 室温通透20 min, 吸除Triton X-100; 取200 μ L罗丹明标记的鬼笔环肽工作液, 覆盖孔中细胞, 室温避光孵育30 min; 置于高内涵细胞分析仪Operetta, 选择“Calculate Texture Properties”分析系统观察, 然后选择“SER features”“Haralick features”“Gabor features”分析每个细胞骨架排列情况。

1.3.8 细胞免疫荧光法: 将6组心肌细胞接种到96孔板中, 3×10^4 孔, 4%多聚甲醛固定10 min, PBS (用0.5% Triton X-100 配制) 清洗3次; 室温通透20 min, 吸除Triton X-100; 每孔加入100 μ L 4%山羊血清, 室温封闭30 min; 一抗(1 : 1 000) 4 $^{\circ}$ C孵育过夜; 二抗(1 : 500) 室温孵育60 min; 每孔加入100 μ L DAPI溶液(100 nmol/L) 进行细胞核复染; 高内涵细胞分析仪Operetta观察MURC和RBM20蛋白定位, 定量分析骨架相关蛋白(β -tubulin和Vinculin) 和极性蛋白(Part6) 的荧光强度, 选择“Calculate Morphology Properties”定量分析肌节蛋白成分-肌球蛋白轻链2(Mlc-2v) 呈现的细胞轮廓来计算细胞表面积。细胞增殖活性用Ki-67标记的红色荧光与DAPI标记的细胞总数比值来表示。

1.4 统计学分析

采用Graph Pad Prism 9.3.1软件进行统计分析, 符合正态分布的计量资料采用 $\bar{x} \pm s$ 表示, 多组间比较采用单因素方差分析。采用双侧检验, $P < 0.05$ 为差异有统计学意义。

2 结果

2.1 基因突变型心肌细胞构建

通过慢病毒载体将野生和突变质粒感染人心肌细胞AC16构建过表达突变模型。Sanger测序结果与目的DNA序列比对一致。

检测6组心肌细胞中RBM20、MURC mRNA和蛋白表达水平。与Control组和Blank组比较, RBM20 MU+MURC MU组RBM20、MURC mRNA和蛋白表达升高(均 $P < 0.05$); MURC MU+RBM20 WT组MURC mRNA和蛋白表达升高(均 $P = 0.000 1$); RBM20 MU+MURC WT组RBM20 mRNA和蛋白表达升高(均 $P < 0.05$)。与野生组比较, RBM20 MU+MURC MU组RBM20、MURC mRNA和蛋白表达下降(均 $P < 0.05$); MURC MU+RBM20 WT组MURC mRNA和蛋白表达下降(均 $P < 0.05$); RBM20 MU+MURC WT组RBM20 mRNA和蛋白表达下降(均 $P < 0.01$), 见图1。

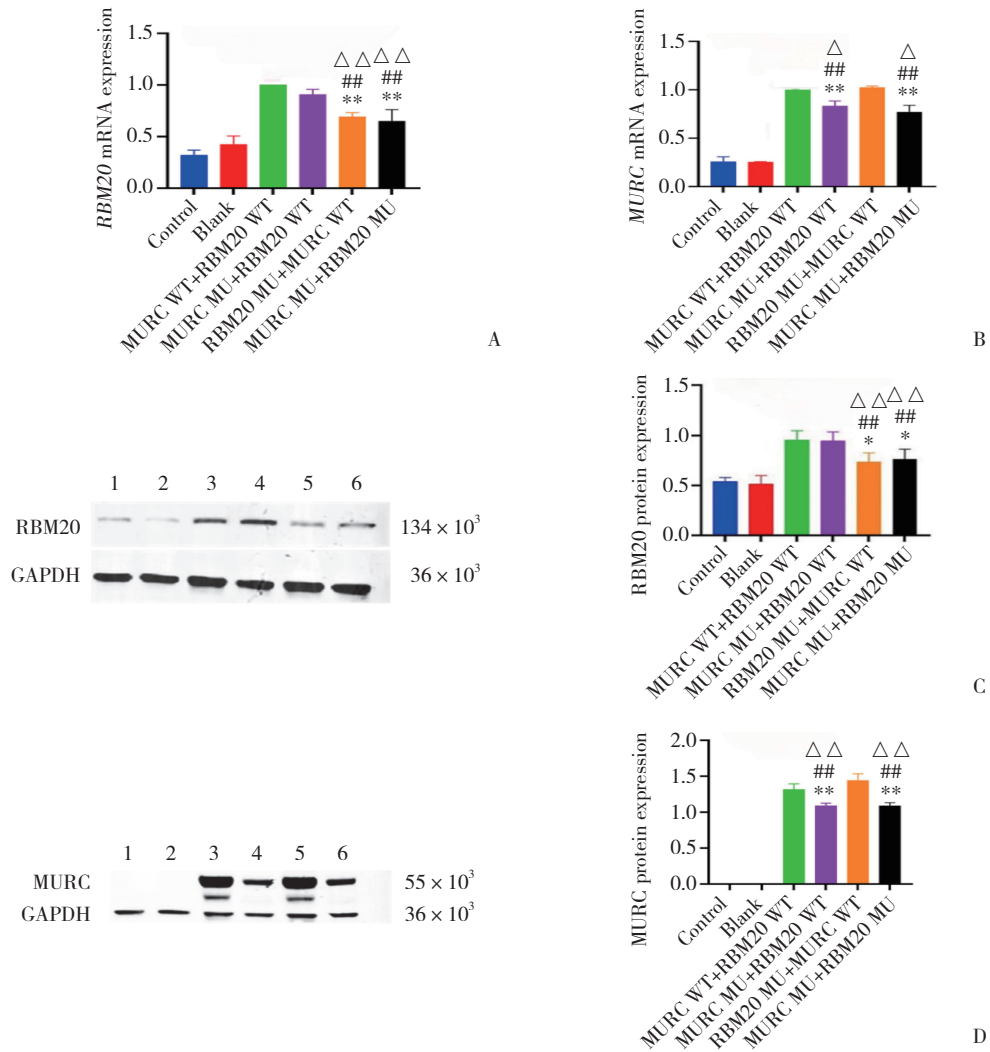
2.2 RBM20和MURC在心肌细胞中的定位

高内涵镜下显示AC16细胞呈绿色荧光, 细胞核呈红色。Control组、Blank组和MURC WT+RBM20 WT组MURC定位于细胞膜, MURC MU+RBM20 WT组、RBM20 MU+MURC WT组、MURC MU+RBM20 MU组MURC定位于细胞质。6组细胞中RBM20均位于细胞核, 见图2。

在分离细胞核及细胞质后进一步验证RBM20和MURC在细胞不同部位的定量表达情况, Western blotting检测结果显示, RBM20蛋白在6组中均仅在细胞核内表达, 在细胞质中几乎无表达。与MURC WT+RBM20 WT组比较, MURC MU+RBM20 WT组、MURC MU+RBM20 MU组细胞膜中MURC蛋白表达下降(P 分别为0.037 1、0.000 1), 而细胞质中MURC蛋白表达上升(P 分别为0.008 7、0.026 8), 见图3。

2.3 RBM20和MURC双基因突变对心肌细胞形态结构的影响

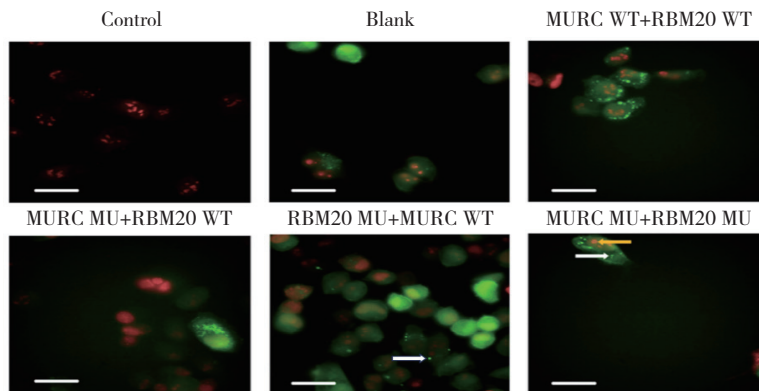
免疫荧光染色显示细胞形态并测定细胞表面积, 与MURC WT+RBM20 WT组比较, MURC MU+RBM20 WT组、RBM20 MU+MURC WT组细胞表面积略增大, 但差异无统计学意义(P 分别为0.927 1、0.120 5); 与MURC WT+RBM20 WT组、MURC MU+RBM20 WT组、RBM20 MU+MURC WT组比较, MURC MU+RBM20 MU组细胞表面积增大(均 $P < 0.05$), 见图4。



A, relative expression level of *RBM20* mRNA; B, relative expression of *MURC* mRNA; C, *RBM20* protein expression; D, *MURC* protein expression. 1, control; 2, blank; 3, *MURC* WT+*RBM20* WT; 4, *MURC* MU+*RBM20* WT; 5, *RBM20* MU+*MURC* WT; 6, *MURC* MU+*RBM20* MU. Compared with control group, * $P < 0.05$, ** $P < 0.01$; compared with blank group, ## $P < 0.01$; compared with *MURC* WT+*RBM20* WT group, $\Delta P < 0.05$, $\Delta\Delta P < 0.01$.

图1 *RBM20*和*MURC* mRNA和蛋白表达

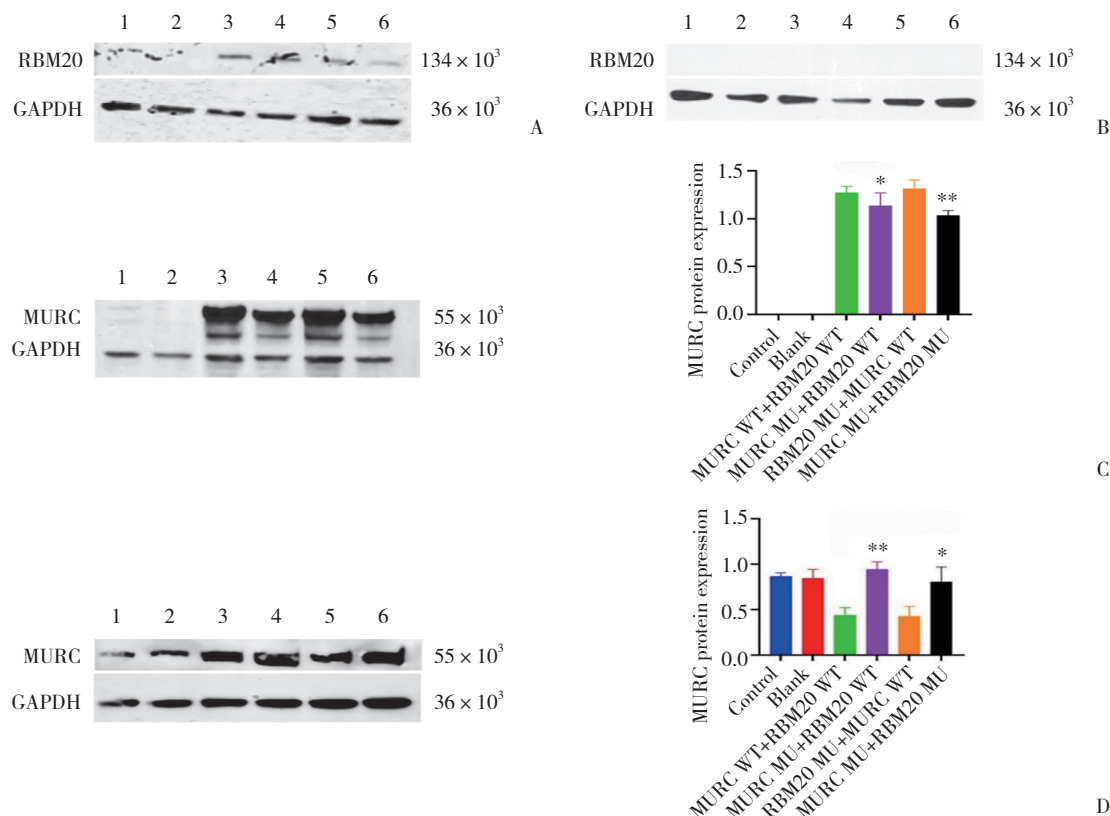
Fig.1 *RBM20* and *MURC* mRNA and protein expression



RBM20, red fluorescence; *MURC*, bright green fluorescence; cells transfected with the lentiviral vector, green fluorescence. Orange arrows indicate the localization of *RBM20* in the cell after mutation of *RBM20* and *MURC*. The white arrow indicates the localization of *MURC* fusion proteins in the cell. Scale bar=50 μm .

图2 各组心肌细胞内*RBM20*和*MURC*定位情况

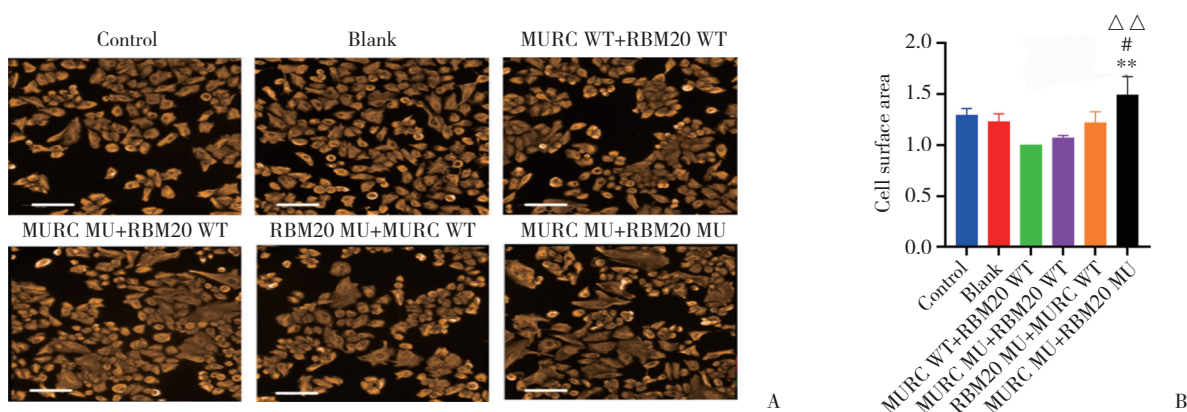
Fig.2 Localization of *RBM20* and *MURC* in cardiomyocytes of each group



A, RBM20 protein expression in the nucleus; B, RBM20 protein expression in the cytoplasm; C, MURC protein expression on cell membrane; D, MURC protein expression in the cytoplasm. 1, control; 2, blank; 3, MURC WT+RBM20 WT; 4, MURC MU+RBM20 WT; 5, RBM20 MU+MURC WT; 6, MURC MU+RBM20 MU. Compared with MURC WT+RBM20 WT group, * $P < 0.05$, ** $P < 0.01$.

图3 各组细胞核/细胞质内RBM20和MURC蛋白表达水平

Fig.3 Protein expression levels of RBM20 and MURC in the nucleus or cytoplasm in each group



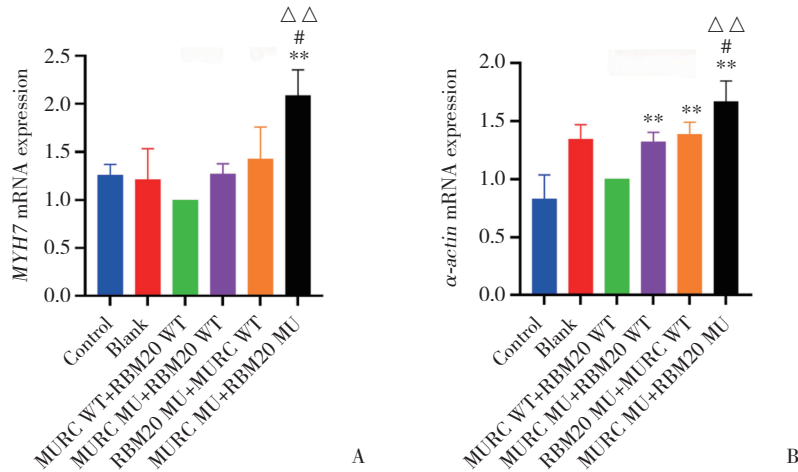
A, immunofluorescence staining of Mlc-2v in cardiomyocytes; B, myocardial cell surface area. Mlc-2v, orange-red fluorescence. Scale bar = 200 μm . Compared with MURC WT+RBM20 WT group, ** $P < 0.01$; compared with MURC MU+RBM20 WT group, $\Delta\Delta P < 0.01$; compared with RBM20 MU+MURC WT group, # $P < 0.05$.

图4 细胞免疫荧光显示各组心肌细胞表面积情况

Fig.4 Cardiomyocyte area in each group as determined by immunofluorescence

与MURC WT+RBM20 WT组比较, MURC MU+RBM20 WT组、RBM20 MU+MURC WT组 α -actin mRNA表达升高(均 $P = 0.0001$); 而 β -肌球蛋白重链(myosin heavy chain 7, MYH7) mRNA表达略升高, 但差异无

统计学意义(P 分别为0.5871、0.1690)。与MURC WT+RBM20 WT组、MURC MU+RBM20 WT组、RBM20 MU+MURC WT组比较, MURC MU+RBM20 MU组MYH7、 α -actin mRNA表达均显著升高(均 $P < 0.05$), 见图5。



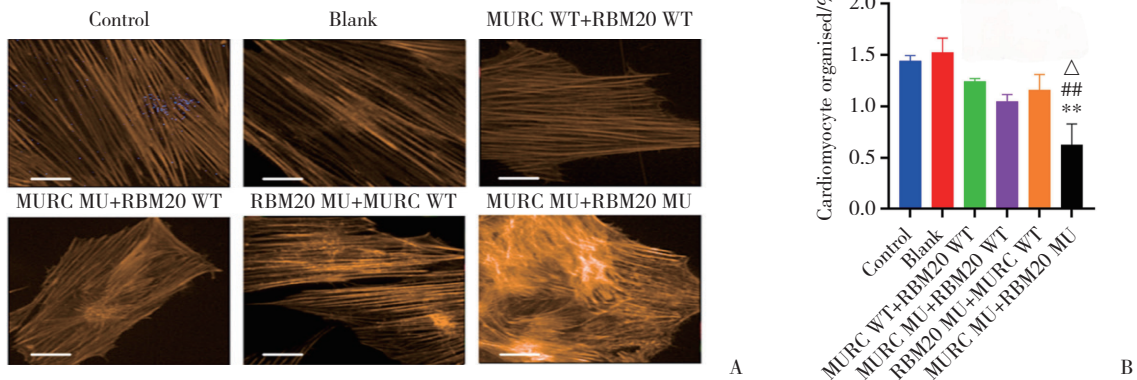
A, relative expression level of MYH7 mRNA; B, relative expression level of α -actin mRNA. Compared with MURC WT+RBM20 WT group, $**P < 0.01$; compared with MURC MU+ RBM20 WT group, $\Delta \Delta P < 0.01$; compared with RBM20 MU+MURC WT group, $\#P < 0.05$.

图5 实时荧光定量PCR检测各组MYH7、 α -actin mRNA表达

Fig.5 mRNA expression of MYH7 and α -actin as detected by RT-qPCR

细胞免疫荧光检测心肌细胞骨架形态(疏密、紊乱度)结果显示, MURC WT+RBM20 WT组细胞骨架排列疏松, 纹理和走向清晰; 而MURC MU+RBM20 WT组、RBM20 MU+MURC WT组、RBM20 MU+MURC WT组细胞骨架纹理发生重排, 走向不清晰, 见图6A。与MURC WT+RBM20 WT组比较, MURC MU+

RBM20 WT组、RBM20 MU+MURC WT组细胞骨架排列整齐度有下降趋势, 但差异无统计学意义(P 分别为0.626 4、0.940 8)。与MURC WT+RBM20 WT组、MURC MU+ RBM20 WT组、RBM20 MU+MURC WT组比较, MURC MU+RBM20 MU组细胞骨架排列整齐度均下降(均 $P < 0.05$), 见图6B。



A, myocardial cytoskeleton immunofluorescence staining, F-actin labeled cytoskeleton, orange-red fluorescence (Scale bar = 25 μ m); B, the results of myocardial cytoskeletal arrangement. Compared with MURC WT+RBM20 WT group, $**P < 0.01$; compared with MURC MU+RBM20 WT group, $\Delta P < 0.05$; compared with RBM20 MU+MURC WT group, $##P < 0.01$.

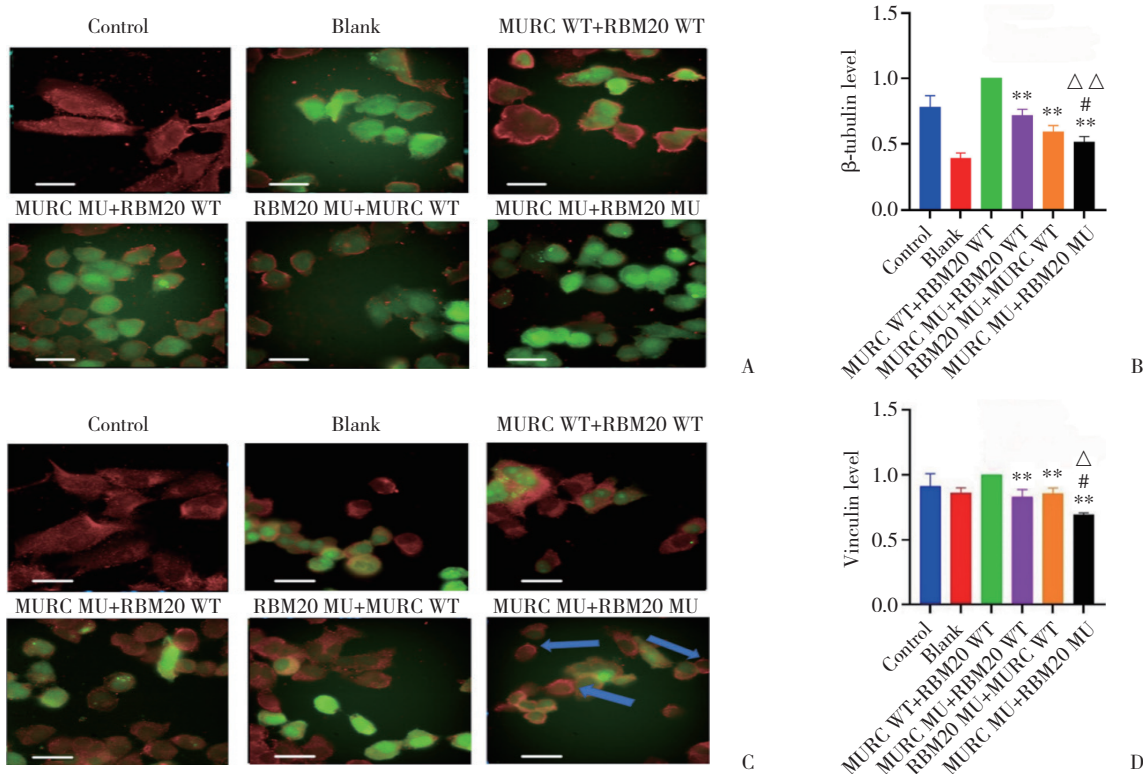
图6 各组心肌细胞骨架的排列情况

Fig.6 The arrangement of the myocardial cytoskeleton in each group

结果显示, 各组细胞内 β -tubulin呈散在分布, 多见于细胞膜。MURC WT+RBM20 WT组、MURC MU+RBM20 WT组、RBM20 MU+MURC WT组细胞中Vinculin分布较均匀, 而MURC MU+RBM20 MU组细胞膜上Vinculin浓聚, 细胞质中分布较少, 明显分布不均。与MURC WT+RBM20 WT组比较, MURC MU+RBM20

WT组、RBM20 MU+MURC WT组 β -tubulin和Vinculin荧光强度均下降(均 $P < 0.05$), 见图7。

与MURC WT+RBM20 WT组、MURC MU+ RBM20 WT组、RBM20 MU+MURC WT组比较, MURC MU+RBM20 MU组 β -tubulin和Vinculin荧光强度均下降(均 $P < 0.05$), 见图7。



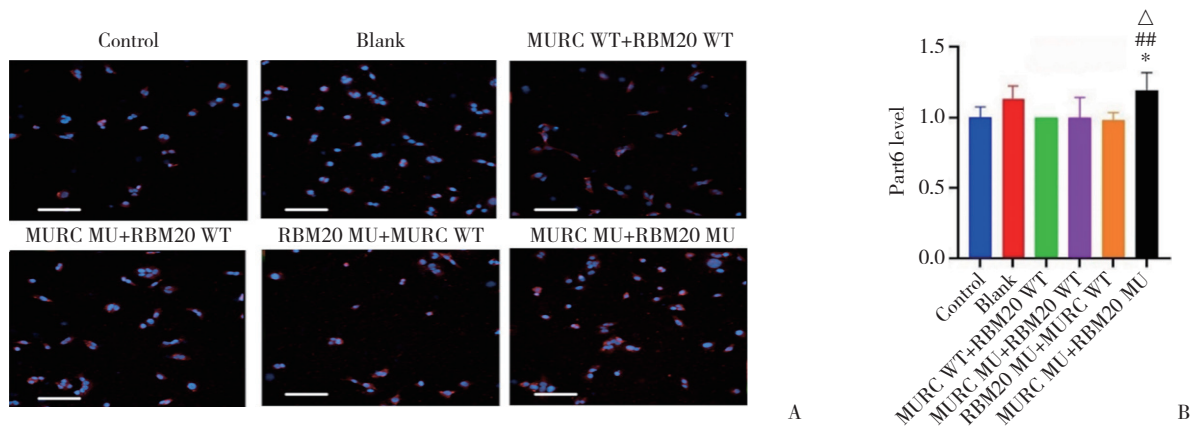
A, immunofluorescence staining of skeleton protein β-tubulin (β-tubulin, red; cells, green. Scale bar = 50 μm); B, relative fluorescence intensity of skeleton protein β-tubulin; C, immunofluorescence staining of skeleton protein Vinculin (Vinculin, red; cells, green. The blue arrows indicate the distribution of Vinculin after mutations in both RBM20 and MURC. Scale bar = 50 μm); D, relative fluorescence intensity of skeleton protein Vinculin. Compared with MURC WT+RBM20 WT group, * $P < 0.05$, ** $P < 0.01$; compared with MURC MU+RBM20 WT group, $\Delta P < 0.05$, $\Delta \Delta P < 0.01$; compared with RBM20 MU+MURC WT group, # $P < 0.05$.

图7 各组骨架蛋白β-tubulin和Vinculin的荧光强度比较

Fig.7 Comparison of fluorescence intensity of skeleton protein β-tubulin and Vinculin in each group

结果显示,各组细胞细胞核及细胞质中极性蛋白Part6均散在分布。与MURC WT+RBM20 WT组相比,MURC MU+RBM20 WT组、RBM20 MU+MURC WT组Part6荧光强度有上升趋势,但差异无统计学意

义(P 分别为0.983 3、0.990 2)。与MURC WT+RBM20 WT组、MURC MU+RBM20 WT组、RBM20 MU+MURC WT组比较,MURC MU+RBM20 MU组Part6荧光强度均上升(均 $P < 0.05$),见图8。



A, polar protein Part6 immunofluorescence staining (Part6, red; nucleus, blue. Scale bar = 200 μm); B, relative fluorescence intensity of polar protein Part6. Compared with the MURC WT+RBM20 WT group, * $P < 0.05$; compared with MURC MU+RBM20 WT group, $\Delta P < 0.05$; compared with RBM20 MU+MURC WT group, ## $P < 0.01$.

图8 各组极性蛋白Part6的荧光强度

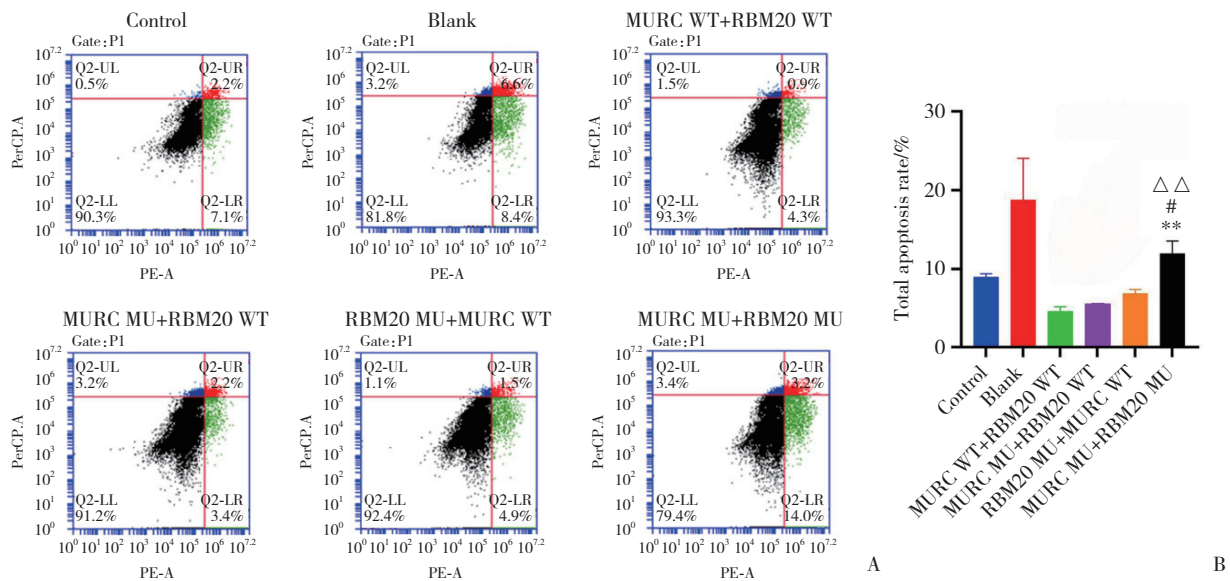
Fig.8 Fluorescence intensity of polar protein Part 6 in each group

2.4 *RBM20*和*MURC*双基因突变对心肌细胞生物学特性的影响

流式细胞术检测显示,与MURC WT+RBM20 WT组比较,MURC MU+RBM20 WT组、RBM20 MU+MURC WT组凋亡率均有上升趋势,但无统计学差异(均 $P > 0.05$)。与MURC WT+RBM20 WT组、MURC MU+RBM20 WT组、RBM20 MU+MURC WT组比较,MURC MU+RBM20 MU组凋亡率均上升(均 $P < 0.05$),见图

9。

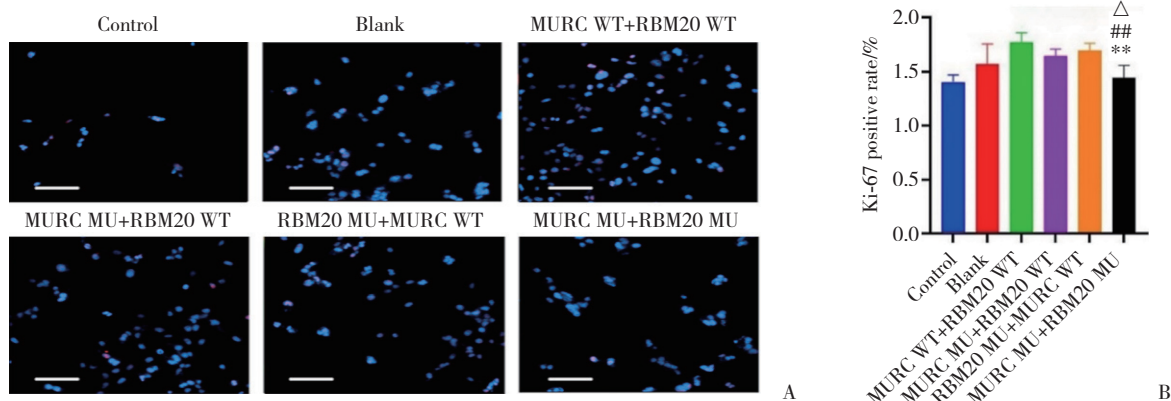
Ki-67染色观察心肌细胞增殖情况,与MURC WT+RBM20 WT组比较,MURC MU+RBM20 WT组、RBM20 MU+MURC WT组增殖率略下降,但差异无统计学意义(P 分别为0.3329、0.8179)。与MURC WT+RBM20 WT组、MURC MU+RBM20 WT组、RBM20 MU+MURC WT组比较,MURC MU+RBM20 MU组增殖率下降(均 $P < 0.05$),见图10。



A, flow cytometry was used to detect cell apoptosis. The black scatter in the lower left quadrant represents the proportion of living cells; the green scatter in the lower right quadrant represents the proportion of cells at the early stage of apoptosis; the blue scatter in the upper left quadrant represents the proportion of cells damaged by improper operation; the red dot in the upper right quadrant represents the proportion of cells in late apoptosis. B, cell apoptosis rate (early apoptosis ratio+late apoptosis ratio). Compared with MURC WT+RBM20 WT group, $**P < 0.01$; compared with MURC MU+RBM20 WT group, $\Delta\Delta P < 0.01$; compared with RBM20 MU+MURC WT group, $\#P < 0.05$.

图9 流式细胞术显示各组心肌细胞凋亡情况

Fig.9 Apoptosis of cardiomyocytes in each group as determined by flow cytometry



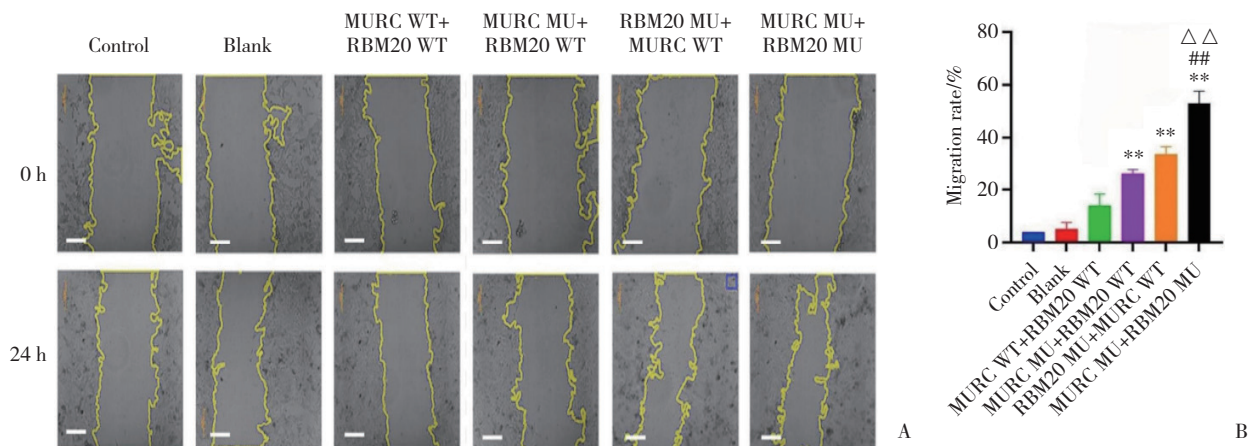
A, immunofluorescence staining of proliferating cells (Ki-67 labeled proliferative cells are red, and all cell nuclei are blue. Scale bar = 200 μm); B, Ki-67 positive rate (cardiomyocyte proliferation). Compared with MURC WT+RBM20 WT group, $**P < 0.01$; compared with MURC MU+RBM20 WT group, $\Delta P < 0.05$; compared with RBM20 MU+MURC WT group, $\#\#P < 0.01$.

图10 免疫荧光显示各组心肌细胞增殖情况

Fig.10 Cardiomyocyte proliferation detected by immunofluorescence staining in each group

划痕实验结果显示,与MURC WT+RBM20 WT组比较,MURC MU+RBM20 WT组、RBM20 MU+MURC WT组迁移率均上升(均 $P < 0.05$)。与MURC WT+

RBM20 WT组、MURC MU+RBM20 WT组、RBM20 MU+MURC WT组比较,MURC MU+RBM20 MU组迁移率均上升(均 $P < 0.05$),见图11。



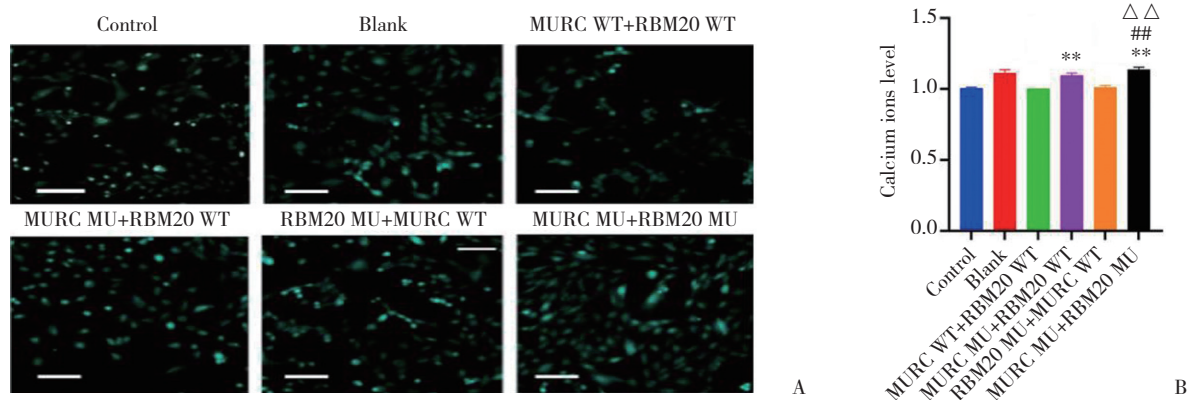
A, scratch test to observe cell migration (scale bar = 200 μ m); B, myocardial cell mobility (percentage of healed area). Compared with MURC WT+RBM20 WT group, $**P < 0.01$; compared with MURC MU+RBM20 WT group, $\Delta\Delta P < 0.01$; compared with RBM20 MU+MURC WT group, $##P < 0.01$.

图11 划痕实验检测各组心肌细胞迁移情况

Fig.11 Cardiomyocyte migration in each group detected by the scratch test

Fura-2-AM标记 Ca^{2+} 染色结果显示,与MURC WT+RBM20 WT组比较,MURC MU+RBM20 WT组 Ca^{2+} 荧光强度升高($P = 0.0001$);而RBM20 MU+MURC WT组 Ca^{2+} 荧光强度略升高,但差异无统计学意义($P =$

0.9999);与MURC WT+RBM20 WT组、MURC MU+RBM20 WT组、RBM20 MU+MURC WT组比较,MURC MU+RBM20 MU组 Ca^{2+} 荧光强度均升高(均 $P < 0.05$),见图12。



A, fluorescence staining of intracellular calcium ions labeled by Fura 2 (green, calcium ion. Scale bar = 100 μ m); B, relative fluorescence intensity of calcium ions. Compared with MURC WT+RBM20 WT group, $**P < 0.01$; compared with MURC MU+RBM20 WT group, $\Delta\Delta P < 0.01$; compared with RBM20 MU+MURC WT group, $##P < 0.01$.

图12 各组心肌细胞内Fura 2-AM荧光强度比较

Fig.12 Comparison of fluorescence intensity of Fura 2-AM in each group

3 讨论

近期研究^[8-9]表明,扩张型心肌病与RBM20突

变相关,一些直接受RBM20调节的基因靶点,如肌钙蛋白T2 (troponin T2, *TNNT2*)、肌联蛋白 (titin, *TTN*) 基因均与心肌扩张表型相关,体外细胞学

表现为心肌细胞表面积增大。本研究结果显示, *RBM20* MU+*MURC* WT组心肌细胞表面积大于*MURC* WT+*RBM20* WT组,但差异无统计学意义($P > 0.05$)。此外,有研究^[10]报道,*RBM20*错义突变的心肌细胞可出现 α -辅肌动蛋白异常分布,表现为骨架结构紊乱,骨架结构畸变,可以部分解释扩张型心肌病的的心脏扩大以及与*TTN*亚型N2BA的保留相关,较大的N2BA亚型可影响Frank-Starling机制,导致心肌粗细肌丝重叠,骨架结构重排。本研究结果显示,与*MURC* WT+*RBM20* WT组相比,*RBM20* MU+*MURC* WT组骨架纹理出现重排,走向不清晰,但差异无统计学意义,这可能是由于双基因突变相互作用导致心肌细胞结构异常更显著,*RBM20*和*MURC*基因之间可能通过*TTN*和*CAV3*基因介导相互作用,对后两者的生物学过程富集分析提示其参与心肌细胞内肌节Z线的形成,可能最终影响心肌细胞结构和功能^[11-12]。

*RBM20*突变引起的心肌病可以通过改变钙调蛋白依赖性蛋白激酶 II delta (calmodulin-dependent protein kinase type II subunit delta, Camk2d) 同构体CaMK II δ A和CaMK II δ 9的剪切进而损害Camk2d;持续存在的Camk2d未剪切形式与扩张性心肌病的电生理表型改变相关,表现为细胞钙处理能力改变,以细胞钙过载为标志,且舒张期细胞内Ca²⁺升高,峰值瞬态增加^[13-14]。这些研究均提示*RBM20*突变可能引起心肌细胞钙相关电生理和功能改变。本研究结果显示,与*MURC* WT+*RBM20* WT组相比,*RBM20* MU+*MURC* WT组心肌细胞钙处理能力下降,但差异无统计学意义。然而,*RBM20*与*MURC*双基因突变影响了细胞内Ca²⁺浓度。以往研究^[15]提示,*MURC*可能通过与*STIM1*相互作用调节系统操作Ca²⁺进入细胞。同时,*RBM20*突变的靶标CaMK II δ 调节肥厚心肌细胞中*STIM1*的表达^[16],因此推测*RBM20*和*MURC*双基因突变可能通过影响*STIM1*来进一步调节心肌细胞钙处理能力。

*MURC*基因具有2个卷曲螺旋结构域HR1和HR2。HR1对*MURC*在心肌细胞中的膜靶向至关重要^[15]。心肌细胞中*MURC*定位于细胞膜,而缺乏螺旋结构域的*MURC*突变体主要定位于细胞质。本研究中*MURC* MU+ *RBM20* WT组*MURC*分布于整个细胞质中,不再局限于细胞膜,证实了突变型*MURC*可能由

于改变HR1最终导致其定位发生改变。HR1缺失型突变的*MURC*与野生型*MURC*相比,表达出更高水平的肥大相关基因。*MURC*缺失突变会诱导 α 1肾上腺素能受体/ERK通路激活和肥大反应^[17],在 α 1肾上腺素能受体的刺激下,*MURC*缺失突变小鼠表现出心脏肥大逆转,并伴有ERK激活抑制。本研究表明确实*MURC*单基因突变后 α -actin mRNA表达升高,提示心肌细胞表面积增大。因此,推测本研究中*MURC* (c.71A>T)可能通过抑制 α 1肾上腺素能受体激活引起心脏肥大,表现为心肌细胞表面积增大。但是否存在其他影响心肌细胞肥大的通路需进一步研究论证。

心肌致密化不全是一种遗传性多基因心肌病^[18],这些基因主要编码参与细胞骨架、肌节、线粒体和离子通道的蛋白质^[19]。有研究^[20]发现细胞骨架调控心肌细胞膜上黏着斑蛋白的重分布,可触发肌小梁分层,证明细胞骨架参与了心肌肌小梁的形成。随着心肌细胞进一步分化、增殖和延伸,形成突出的小梁,促进了心肌中氧气和营养物质的交换。本研究发现心肌细胞发生*RBM20*和*MURC*特定位点突变后,细胞骨架排列紊乱、凋亡率明显升高,增殖活性下降以及迁移率增高。微管作为细胞骨架的重要组成部分,具备多种生物学功能。微管蛋白则是微管的关键组成成分,其中 β -tubulin作为异二聚体微管蛋白可与核苷酸分子结合,与GTP结合时可组装成微管,而与GDP结合时可分裂微管^[21]。而Vinculin是广泛表达的细胞骨架蛋白,沿肌动蛋白丝排列^[22]。同时可将细胞骨架固定在细胞外基质上,而细胞外基质在心脏发育的致密化过程中起促进作用^[23]。本研究发现当心肌细胞发生*RBM20*和*MURC*双基因突变后微管蛋白 β -tubulin发生改变,通过影响微管的动态平衡,从而影响细胞骨架排列的疏密和紊乱度;而Vinculin分布发生改变,可通过影响骨架的固定最终导致NVM。

此外,细胞极性蛋白在小鼠心室肌小梁形态发生过程的定向细胞分裂中是必不可少的^[24]。JIMÉNEZ-AMILBURU等^[25]在斑马鱼的研究中也证明极性蛋白的缺失可能造成心室肌小梁分层失败。Part6作为细胞极性蛋白之一,参与不对称细胞分裂和细胞极化过程,进而影响细胞迁移^[26]。小鼠心肌细胞研究^[27]也表明增加心室发育过程中心肌细

胞肌原纤维生成缺陷和极化可能是NVM的常见致病途径。本研究发现当心肌细胞发生双重基因突变后,Part6荧光强度上升且心肌细胞迁移能力增强。因此推测*RBM20*和*MURC*发生此特定位点杂合突变后,通过改变细胞极性,影响了细胞迁移能力。HIRONO等^[28]研究表明,增殖和分化过程紊乱以及拉伸不耐受可能是NVM的基础。1项关于*eIF3a*基因突变的研究^[29]表明小鼠心肌细胞可通过诱导凋亡来降低增殖能力。本研究也发现当心肌细胞发生双重基因突变后,心肌细胞增殖能力下降,凋亡率升高。因此,推测*MURC*和*RBM20*发生双重突变后心脏非致密化组织的出现很可能是诱导细胞凋亡而降低了心肌细胞增殖能力所致。

综上所述,*RBM20*和*MURC*双基因杂合变异可使心肌细胞的形态结构和生物学特性发生改变,表现为表面积增大,细胞骨架排列紊乱,骨架相关蛋白表达量下降,极性改变;心肌细胞凋亡率升高,增殖活性降低,迁移率升高,钙处理能力降低。本研究仅在体外实验提示了*RBM20*和*MURC*双基因杂合变异对心肌细胞形态和功能的影响,而体内实验需利用双基因突变动物模型来进一步验证。此外,尽管本研究提示*RBM20*和*MURC*双基因突变提高了细胞内Ca²⁺浓度,但尚未阐述其可能的电生理影响,今后需应用膜片钳和光电标测等方法进一步探讨双基因突变对心肌细胞电信号传导及兴奋收缩耦联的作用。

参考文献:

- [1] 李秋雨. *RBM20*和*MURC*基因罕见杂合错义突变致病性分析[D]. 福州:福建医科大学,2021. DOI:10.27020/d.cnki.gfyiu.2021.000047.
- [2] ROJANASOPONDIST P, NESHEIWAT L, PIOMBO S, et al. Genetic basis of left ventricular noncompaction [J]. *Circ Genom Precis Med*, 2022, 15 (3) : e003517. DOI: 10.1161/circgen.121.003517.
- [3] VAKHRUSHEV Y, KOZYREVA A, SEMENOV A, et al. *RBM20*-associated ventricular arrhythmias in a patient with structurally normal heart [J]. *Genes*, 2021, 12 (1) : 94. DOI: 10.3390/genes12010094.
- [4] TIJSEN AJ, CÓCERA ORTEGA L, RECKMAN YJ, et al. Titin circular RNAs create a back-splice motif essential for SRSF10 splicing [J]. *Circulation*, 2021, 143 (15) : 1502-1512. DOI: 10.1161/CIRCULATIONAHA.120.050455.
- [5] LI MM, XIA S, XU L, et al. Genetic analysis using targeted next-generation sequencing of sporadic Chinese patients with idiopathic dilated cardiomyopathy [J]. *J Transl Med*, 2021, 19 (1) : 189. DOI: 10.1186/s12967-021-02832-3.
- [6] SVAHN J, COUDERT L, STREICHENBERGER N, et al. Immune-mediated rippling muscle disease associated with thymoma and anti-*MURC/cavin-4* autoantibodies [J]. *Neurol Neuroimmunol Neuroinflamm*, 2022, 10 (1) : e200068. DOI: 10.1212/NX1.0000000000200068.
- [7] NISHI M, OGATA T, CANNISTRACI CV, et al. Systems network genomic analysis reveals cardioprotective effect of *MURC/cavin-4* deletion against ischemia/reperfusion injury [J]. *J Am Heart Assoc*, 2019, 8 (15) : e012047. DOI: 10.1161/JAHA.119.012047.
- [8] FOCHI S, LORENZI P, GALASSO M, et al. The emerging role of the *RBM20* and *PTBP1* ribonucleoproteins in heart development and cardiovascular diseases [J]. *Genes*, 2020, 11 (4) : 402. DOI: 10.3390/genes11040402.
- [9] GAERTNER A, BLOEBAUM J, BRODEHL A, et al. The combined human genotype of truncating *TTN* and *RBM20* mutations is associated with severe and early onset of dilated cardiomyopathy [J]. *Genes*, 2021, 12 (6) : 883. DOI: 10.3390/genes12060883.
- [10] SCHNEIDER JW, OOMMEN S, QURESHI MY, et al. Dysregulated ribonucleoprotein granules promote cardiomyopathy in *RBM20* gene-edited pigs [J]. *Nat Med*, 2020, 26 (11) : 1788-1800. DOI: 10.1038/s41591-020-1087-x.
- [11] JORDAN E, PETERSON L, AI T, et al. Evidence-based assessment of genes in dilated cardiomyopathy [J]. *Circulation*, 2021, 144 (1) : 7-19. DOI: 10.1161/CIRCULATIONAHA.120.053033.
- [12] WOODMAN SE, PARK DS, COHEN AW, et al. Caveolin-3 knockout mice develop a progressive cardiomyopathy and show hyperactivation of the p42/44 MAPK cascade [J]. *J Biol Chem*, 2002, 277 (41) : 38988-38997. DOI: 10.1074/jbc.M205511200.
- [13] LENNERMANN D, BACKS J, VAN DEN HOOGENHOF MMG. New insights in *RBM20* cardiomyopathy [J]. *Curr Heart Fail Rep*, 2020, 17 (5) : 234-246. DOI: 10.1007/s11897-020-00475-x.
- [14] LIU J, WANG K, LIU XY, et al. *RBM24* controls cardiac QT interval through CaMKII δ splicing [J]. *Cell Mol Life Sci*, 2022, 79 (12) : 613. DOI: 10.1007/s00018-022-04624-4.
- [15] MALETTE J, DEGRANDMAISON J, GIGUÈRE H, et al. *MURC/CAVIN-4* facilitates store-operated calcium entry in neonatal cardiomyocytes [J]. *Biochim Biophys Acta Mol Cell Res*, 2019, 1866 (8) : 1249-1259. DOI: 10.1016/j.bbamer.2019.03.017.
- [16] JI YW, GUO X, ZHANG Z, et al. CaMKII δ mediates phenylephrine induced cardiomyocyte hypertrophy through store-operated Ca²⁺ entry [J]. *Cardiovasc Pathol*, 2017, 27 : 9-17. DOI: 10.1016/j.carpath.2016.11.004.
- [17] OGATA T, NAITO D, NAKANISHI N, et al. *MURC/Cavin-4* facilitates recruitment of ERK to caveolae and concentric cardiac hypertrophy induced by α 1-adrenergic receptors [J]. *Proc Natl Acad Sci USA*, 2014, 111 (10) : 3811-3816. DOI: 10.1073/pnas.1315359111.
- [18] CANNIE D, ELLIOTT P. The genetics of left ventricular noncompaction [J]. *Curr Opin Cardiol*, 2021, 36 (3) : 301-308. DOI: 10.1097/HCO.0000000000000844.
- [19] MCKENNA WJ, JUDGE DP. Epidemiology of the inherited cardiomyopathies [J]. *Nat Rev Cardiol*, 2021, 18 (1) : 22-36. DOI: 10.1038/s41569-020-0428-2.
- [20] GUNAWAN F, PRIYA R, STAINIER DYR. Sculpting the heart: cellular mechanisms shaping valves and trabeculae [J]. *Curr Opin Cell Biol*, 2021, 73 : 26-34. DOI: 10.1016/j.ceb.2021.04.009.
- [21] LAWSON CD, RIDLEY AJ. Rho GTPase signaling complexes in cell migration and invasion [J]. *J Cell Biol*, 2018, 217 (2) : 447-457. DOI: 10.1083/jcb.201612069.

- progesterone and progesterone/estradiol ratio on the hCG trigger day in predicting pregnancy outcomes of PCOS patients undergoing IVF/ICSI: a retrospective cohort study [J]. *Reprod Biol Endocrinol*, 2021, 19 (1) : 184. DOI: 10.1186/s12958-021-00862-6.
- [17] PANWAR M, MOHANTY A, AHUJA N, et al. Maternal β -hCG and neutrophil lymphocyte ratio during pregnancy to predict high-risk neonates: an observational study [J]. *Maedica*, 2022, 17 (2) : 317-322. DOI: 10.26574/maedica.2022.17.2.317.
- [18] 尚聪敏. 盐酸利托君联合地屈孕酮对先兆流产患者血清 β -人绒毛膜促性腺激素、孕酮及雌二醇水平的影响 [J]. *实用临床医药杂志*, 2019, 23 (18) : 122-124, 128. DOI: 10.7619/jcmp.201918035.
- [19] SOYSAL C, SARı H, İŞIKALAN MM, et al. Role of the systemic immune-inflammation index in threatened abortion patients and predicting of abortion [J]. *J Obstet Gynaecol Res*, 2023, 49 (7) : 1723-1728. DOI: 10.1111/jog.15655.
- [20] 张春芳, 王芳, 牟方祥, 等. 免疫因素与绒毛膜下血肿关系的研究进展 [J]. *中国计划生育和妇产科*, 2023, 15 (3) : 32-36. DOI: 10.3969/j.issn.1674-4020.2023.03.07.
- [21] 张泳仪, 莫伟平. 反复自然流产中封闭抗体和抗心磷脂抗体检测的价值 [J]. *深圳中西医结合杂志*, 2021, 31 (8) : 102-103. DOI: 10.16458/j.cnki.1007-0893.2021.08.046.
- [22] GUO X, WANG F, LI J, et al. Prediction performance of serum placental growth factor (PLGF) human chorionic gonadotropin β (β -hCG) and PAPP-a levels in early pregnancy for pregnancy outcomes [J]. *Pak J Med Sci*, 2022, 38 (7) : 1877-1882. DOI: 10.12669/pjms.38.7.5248.
- [23] 李晓莹, 齐红燕, 叶敏. 先兆流产患者血清HLA-G、 β -HCG、PIBF水平与妊娠结局的相关性分析 [J]. *贵州医药*, 2022, 46 (4) : 571-572. DOI: 10.3969/j.issn.1000-744X.2022.04.035.
- [24] 邓飞涛, 欧阳为相, 朱剑文, 等. 早期先兆流产细胞因子的检测及临床价值分析 [J]. *医学分子生物学杂志*, 2019, 16 (5) : 483-486. DOI: 10.3870/j.issn.1672-8009.2019.05.013.
- [25] 林娟, 关红琼, 叶春燕, 等. 盐酸利托君联合硝苯地平对先兆流产患者Th17和Treg细胞的影响 [J]. *中国性科学*, 2019, 28 (6) : 79-82. DOI: 10.3969/j.issn.1672-1993.2019.06.023.
- [26] MURATA T, KYOZUKA H, YASUDA S, et al. Effects of maternal ritodrine hydrochloride administration on the heart rate of preterm fetal sheep with intraamniotic inflammation [J]. *PLoS One*, 2022, 17 (3) : e0265872. DOI: 10.1371/journal.pone.0265872.
- [27] YONAGA Y, ITO A. The safety of ritodrine hydrochloride: adverse effects on fetuses and newborns [J]. *Drug Discov Ther*, 2021, 15 (1) : 14-19. DOI: 10.5582/DDT.2021.01016.

(编辑 武玉欣)

(上接第892页)

- [22] LEE HT, SHAREK L, O'BRIEN ET, et al. Vinculin and metavinculin exhibit distinct effects on focal adhesion properties, cell migration, and mechanotransduction [J]. *PLoS One*, 2019, 14 (9) : e0221962. DOI: 10.1371/journal.pone.0221962.
- [23] PARRA-ACERO H, HARCET M, SÁNCHEZ-PONS N, et al. Integrin-mediated adhesion in the unicellular holozoan *Capsaspora owczarzewski* [J]. *Curr Biol*, 2020, 30 (21) : 4270-4275.e4. DOI: 10.1016/j.cub.2020.08.015.
- [24] WU MF. Mechanisms of trabecular formation and specification during cardiogenesis [J]. *Pediatr Cardiol*, 2018, 39 (6) : 1082-1089. DOI: 10.1007/s00246-018-1868-x.
- [25] JIMÉNEZ-AMILBURU V, STAINIER DYR. The transmembrane protein Crb2a regulates cardiomyocyte apicobasal polarity and adhesion in zebrafish [J]. *Development*, 2019, 146 (9) : dev171207. DOI: 10.1242/dev.171207.
- [26] DICKINSON DJ. Untangling interactions in the PAR cell polarity system [J]. *J Biol Chem*, 2023, 299 (3) : 102947. DOI: 10.1016/j.jbc.2023.102947.
- [27] LIU Y, CHEN HY, SHOU WN. Potential common pathogenic pathways for the left ventricular noncompaction cardiomyopathy (LVNC) [J]. *Pediatr Cardiol*, 2018, 39 (6) : 1099-1106. DOI: 10.1007/s00246-018-1882-z.
- [28] HIRONO K, SAITO K, MUNKHSAIKHAN U, et al. Familial left ventricular non-compaction is associated with a rare p.V407I variant in bone morphogenetic protein 10 [J]. *Circ J*, 2019, 83 (8) : 1737-1746. DOI: 10.1253/circj.CJ-19-0116.
- [29] GE M, BAI XH, LIU AY, et al. An eIF3a gene mutation dysregulates myocardium growth with left ventricular noncompaction via the p-ERK1/2 pathway [J]. *Genes Dis*, 2020, 8 (4) : 545-554. DOI: 10.1016/j.gendis.2020.02.003.

(编辑 武玉欣)